Agricultural Systems 189 (2021) 103040

Contents lists available at ScienceDirect

Agricultural Systems

journal homepage: www.elsevier.com/locate/agsy

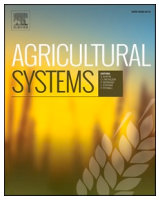

Assessing the vulnerability and risk of maize to drought in China based on the AquaCrop model

Xiufang Zhu [a,b,c], Kun Xu [a,c,*], Ying Liu [a,c], Rui Guo [c], Lingyi Chen [c]

[a] Key Laboratory of Environmental Change and Natural Disaster, Ministry of Education, Beijing Normal University, Beijing 100875, China
[b] State Key Laboratory of Remote Sensing Science, Jointly Sponsored by Beijing Normal University and Institute of Remote Sensing and Digital Earth of Chinese Academy of Sciences, Beijing 100875, China
[c] Institute of Remote Sensing Science and Engineering, Faculty of Geographical Science, Beijing Normal University, Beijing 100875, China

ARTICLE INFO

Keywords:
AquaCrop
Drought
Vulnerability curve
Risk
Yield loss
Maize

ABSTRACT

In the context of global climate change, droughts pose a serious threat to agricultural development and food security. Assessing the vulnerability and risk of regions to drought is important for its prevention. In this paper, to understand the vulnerability of maize to drought in different regions of China and quantify its risk, 241 prefecture-level administrative regions (including prefecture-level cities, autonomous prefectures, prefectures, and leagues) in the five main maize-growing regions of China are used as study area. By using a method of global sensitivity analysis, the extended Fourier amplitude sensitivity test (EFAST), we chose two parameters that are most sensitive to maize yield to calibrate the AquaCrop model. We then used it to simulate the water stress of maize in the study area under different irrigation scenarios as well as the corresponding production. We defined the drought hazard index (DHI) as the daily average of the crop water stress indicator during the growing season, and used it to describe the intensity of droughts. Vulnerability curves (the function of the DHI and rate of yield loss) of the entire growth season and various stages of growth were also formulated. These were used to determine the loss of maize yield under four levels of risk (return periods of 5, 10, 20, and 50 years). The results showed the following: 1) the vulnerability curve of maize for the entire growing season was consistent with logistic function, and the coefficient of determination of the equation of regression was $R^2 = 0.93$. The rate of yield loss began increasing rapidly once the DHI had reached 0.2 and approached its maximum value when the DHI was 0.6. 2) The coefficients of determination of the results of regression in 14 scenarios, in which drought had occurred in different stages of growth, were between 0.28 and 0.92. Drought from the tasseling stage to the milk stage had the most significant negative effect on the maize yield, followed by the seventh leaf stage to the tasseling stage and the sowing stage to the seventh leaf stage. Drought from the milk stage to physiological maturity had the least negative effect on the maize yield. 3) Under all four risk levels, the DHI and the yield loss rate of maize in China decreased from the northwest to the southeast. The Northwest Irrigated Maize Region had the highest drought risk among the five maize-growing regions, followed by the North Spring Maize Region, the Huang-Huai-Hai Summer Maize Region, the South Hilly Maize Region, and the Southwest Mountain Maize Region. 4) The DHI calculated by the average method was more representative than that calculated using the accumulative method.

1. Introduction

Against the backdrop of global climate change, extreme meteorological events have been observed frequently in recent years. Agricultural production is significantly influenced by such events because it is heavily dependent on climatic conditions (Rosenzweig et al., 2014; Xie et al., 2018). According to the Intergovernmental Panel on Climate Change (IPCC), and the Food and Agriculture Organization (FAO) of the United Nations, agriculture is among the industries most vulnerable to climate change (IPCC, 2014; FAO, 2017). Among the most common consequences of climate change (Hanson and Weltzin, 2000; Aherne et al., 2006; Cheng et al., 2016; Gizaw and Gan, 2017; Linares et al.,

* Corresponding author at: Key Laboratory of Environmental Change and Natural Disaster, Ministry of Education, Beijing Normal University, Beijing 100875, China.
E-mail address: 201831051046@mail.bnu.edu.cn (K. Xu).

https://doi.org/10.1016/j.agsy.2020.103040
Received 6 September 2020; Received in revised form 14 December 2020; Accepted 17 December 2020
Available online 19 January 2021

2017; Tietjen et al., 2017), droughts are particularly destructive because of their long duration and complex impacts, and pose a serious threat to global food security (Carrao et al., 2016; Mao et al., 2017; Shi et al., 2018; Ahmadalipour et al., 2019). In the last few decades, droughts have led to the loss of 1820 million Mg of cereal crops (maize, wheat, and rice) worldwide (Lesk et al., 2016). Approximately two billion people have been affected by droughts, which have annually cost 6– 8 billion US dollars since 1900 (FAO, 2013). Research has had shown that the areas suffering extreme drought conditions will increase by 29% in the 21st century, and the frequency and duration of droughts may also increase (Burke et al., 2006; Dai, 2013; Dai et al., 2018; Feng et al., 2019). Therefore, the accurate assessment of the risk of drought is important for the sustainable development of agriculture.

In disaster science, risk is defined as a combination of the possibility of a specific destructive event and its negative effects. It can be described as the expectation of loss based on intensity of the hazard and the vulnerability curve/matrix (UNISDR, 2009). In research on assessing the risk of agricultural droughts, "negative effect" refers to crop yield loss, and the corresponding risk is a function of the intensity of the drought and the vulnerability of the crop to it (Wilhite, 2000). To assess the risk of drought, non-quantitative, semi-quantitative, and quantitative models (Shi, 2011) are used to calculate the level, grade, and value of such risk, respectively. Many researchers have calculated the risk of drought based on vulnerability (Yin et al., 2014; Jia et al., 2016; Yue et al., 2018; Chen et al., 2019; Chou et al., 2019; Zeng et al., 2019).

As a measure of resistance to a hazard, vulnerability plays an important role in research on risk assessment. Early studies on vulnerability assessment were mostly qualitative and descriptive (Wisner, 2004; Birkmann, 2006). With the development of fuzzy mathematics, quantitative evaluation has now become common. The three most commonly used methods are vulnerability assessment based on historical data (Dilley, 2005), indicators (Wu and Wilhite, 2004), and hazard loss curves (Zhu et al., 2020).

Hazard loss curves, or vulnerability curves, were initially used to assess the vulnerability of areas to flood in 1964 (Smith, 1994). In recent decades, they have been widely used in studies on such disasters such as floods (Dutta et al., 2003; Wu et al., 2020; Yang et al., 2020), earthquakes (Singhal and Kiremidjian, 1996; Colombi et al., 2008; Orsini, 2012; Ranjbar and Naderpour, 2020; Shan et al., 2020; Wang et al., 2020c), typhoons (Khanduri and Morrow, 2003; Lee and Rosowsky, 2005; Khajwal and Noshadravan, 2020; Yu et al., 2020), landslides (Bell and Glade, 2004; Galli and Guzzetti, 2007), avalanches (Keylock and Barbolini, 2001; Cappabianca et al., 2008), and hailfall (Hohl et al., 2002). In research on agricultural drought, various models of crop growth are used to simulate the crop yield loss, following which vulnerability curves are drawn. For example, based on an improved Environmental Policy Integrated Climate (EPIC) model, Yin et al. (2014) used the water stress index to construct vulnerability curves for maize drought in 35 countries and regions around the world. Guo et al. (2016) subsequently considered environmental factors in this model and fitted a global three-dimensional (3D) vulnerability surface. Wang et al. (2020a, 2013b) and Yue et al. (2015) separately established regionalized drought vulnerability curves of wheat in China, and Jia et al. (2012), Wang et al. (2019) analyzed the vulnerability of maize. Wei et al. (2019) simulated the vulnerability of summer maize in the Huaibei Plain of China using the cropping system model (CSM) CERES-Maize. Wang et al. (2020c, 2020b) used the Agricultural Production Systems sIMulator (APSIM) model to assess the biophysical vulnerability of wheat in eastern Australia. Models of crop growth have also been widely used in research on the risk of agricultural droughts (Leng and Hall, 2019; Kurniasih and Impron, 2017; Wang et al., 2017; Zhang et al., 2019; Wang et al., 2020c, 2020b). However, previous studies have focused on the entire growing season of crops, and analyses of separate stages of growth are rare. In addition, the drought hazard index (DHI) has been

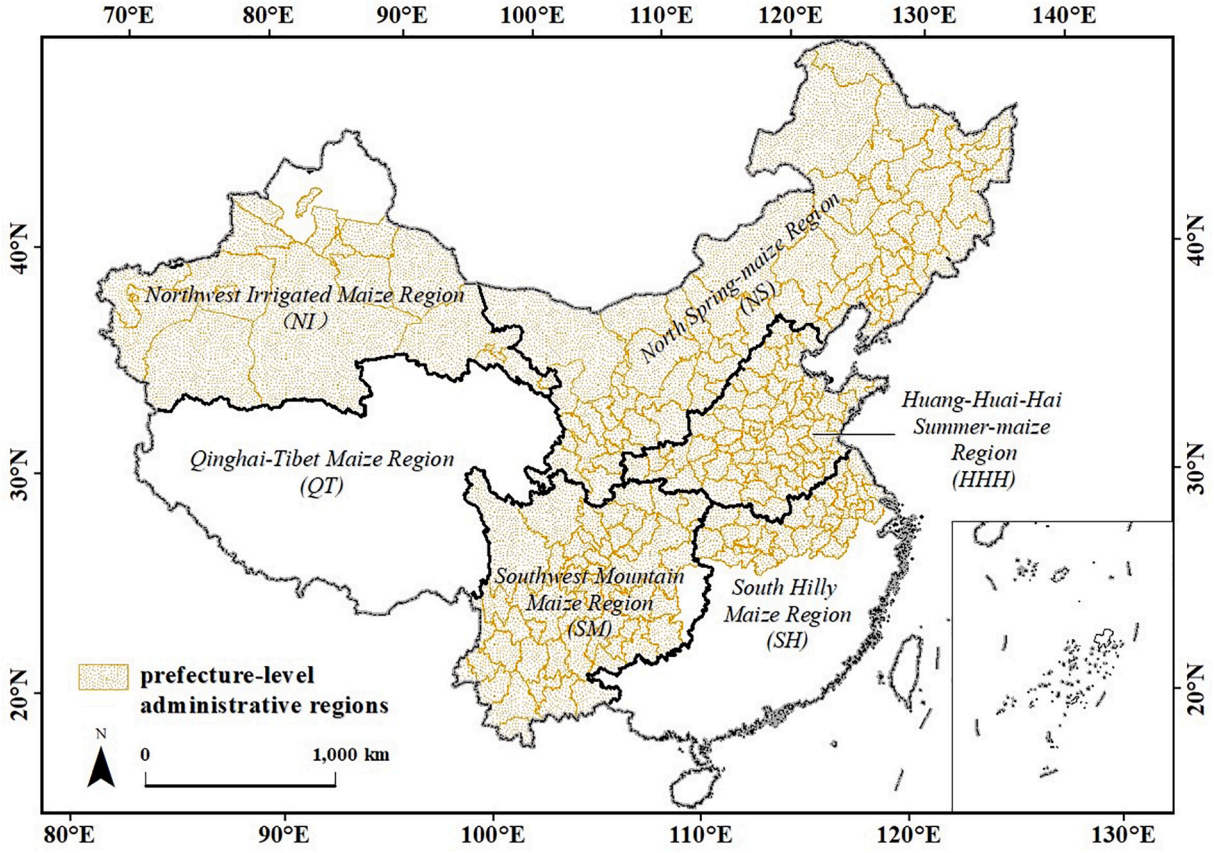

Fig. 1. Study area.

Table 1
Data and sources.

Data Type	Dataset	Data Source	Content	Resolution	Period
Meteorological data	CN05.1	China Meteorological Administration	Precipitation (Daily)	0.25 degrees	1979–2015
	ERA Interim Daily	European Centre for Medium-Range Weather Forecasts(ECMWF) (https://www.ecmwf.int/)	Maximum temperature; Minimum temperature; Mean windspeed; Relative humidity; Surface net solar radiation. (Daily)	0.125 degrees	
Soil data	WISE30sec, v1.0	ISRIC-World Soil Information (http://www.isric.org/)	Soil texture (sand content, silt content and clay content); organic content (7 layers)	30 s	2016
Crop data	Decade Dataset of Crop Growth and Development and Soil Moisture in China	National Meteorological Information Center (http://data.cma.cn/)	Crop growth season	Station	2005–2012
	Harvested Area and Yield for 175 Crops year 2000	EarthStat (http://www.earthstat.org/)	Average crop yield and harvested area	30 s	1997–2003
	Main Crop Yield and Sown Area	China Rural Statistical Yearbook (http://data.cnki.net/)	Maize yield and sown area	Prefecture-level administrative regions	2002–2011

built primarily by using the cumulative values of daily water stress during the growing season. These methods ignore the scenario where extreme drought events can cause crops to die before the end of the growing season.

In this paper, we consider 241 prefecture-level regions of five main maize-growing regions in China as study area, and use the AquaCrop model to simulate maize yield in both rain-fed and irrigation scenarios. Vulnerability curves of maize were constructed and used to evaluate the risk of drought in each region. To solve the problems mentioned above, we propose a method that uses a daily average value instead of the cumulative value to construct the DHI. We also identify the drought-sensitive period of maize by analyzing its vulnerability to drought in various stages of growth.

2. Materials and methods

2.1. Study area

As one of the three main cereal crops in China, maize is grown mainly in the northeast, north, and southwest, forming a long oblique belt from the northeast to the southwest. According to such geographical as climate, soil, landforms, and cropping systems, China can be divided into six main maize-growing regions: the North Spring Maize Region (NS), Huang-Huai-Hai Summer Maize Region (HHH), Southwest Mountain Maize Region (SM), South Hilly Maize Region (SH), Northwest Irrigated Maize Region (NI), and Qinghai–Tibet Maize Region (QT) (Tong, 1992).

The North Spring Maize Region has a humid climate in a cold temperate zone. The region includes Inner Mongolia, Ningxia, Heilongjiang, Jilin, Liaoning, much of Shanxi Province, and parts of Hebei, Shaanxi, and Gansu. Both the temperature and sunlight are moderate. The total annual precipitation is 400–800 mm, mostly concentrated in July to September, which aligns with the season of maize growth. The area of maize planting in this region accounts for 30% of that in China. The Huang-Huai-Hai Summer Maize Region is in a warm temperate and semi-humid zone. It is south of the North Spring Maize Region, and includes Shandong, Henan, much of Hebei Province, and parts of Shanxi, Shaanxi, and Jiangsu. It has a higher temperature and gets more rainfall than the North Spring Maize Region. The Southwest Mountain Maize Region has a semi-humid climate, and includes Sichuan, Yunnan, Guizhou, Chongqing, and parts of Shaanxi, Guangxi, Hubei, Hunan, and Gansu. The annual precipitation is 800–1200 mm, mostly concentrated in April–October. Both heat and water are adequate for crop growth, but the amount of sunlight and quality of soil are poor. The maize planting area in this region accounts for 20% of the total planting area in China. The South Hilly Maize Region has a humid climate in both the subtropical and the tropical zones, and includes Guangdong, Hainan, Fujian, Zhejiang, Jiangxi, Taiwan, and parts of Jiangsu, Anhui, Guangxi, Hunan, and Hubei. The region receives significant precipitation, and is the main rice-producing area of China. The maize planting area accounts for 5% of the country's total maize planting area. The Northwest Irrigated Maize Region includes Xinjiang and much of Gansu Province; it has a continental, arid climate with higher temperatures and abundant sunlight. But the total annual precipitation is less than 200 mm, and agriculture production is dependent on irrigation. The maize planting area accounts for 2% ~ 3% of that of China. The Qinghai-Tibet Maize Region includes Qinghai and Tibet, and is an important pastoral and forest area of China. Its maize planting area accounts for less than 1% of the country's total because of its cold plateau climate.

Using data on the global distribution of crop yield provided by EarthStat, we chose 241 prefecture-level administrative regions in the five main maize-growing regions of China as the study area: 73 in the North Spring Maize Region, 66 in the Huang-Huai-Hai Summer Maize Region, 52 in the Southwest Mountain Maize Region, 34 in the South Hilly Maize Region, and 16 in the Northwest Irrigated Maize Region. The Qinghai-Tibet Maize Region was ignored because of its low production (Fig. 1).

2.2. Models and inputs

AquaCrop is a model of crop growth developed by the FAO to assess the effects of the environment and its management on production. The model consists of three basic modules: those to determine the soil-water balance, simulate crop growth, and the atmospheric composition (Foster et al., 2017).

Crop models can be classified into three main categories based on the core growth engines (Steduto, 2003). AquaCrop is a water-driven model (Todorovic et al., 2009) that impacts crop yields by controlling the available water content in the soil (Steduto et al., 2009). Therefore, compared with light-driven models such as the CERES series (Jones et al., 2003) and carbon-driven models such as WOFOST (Diepen et al., 1989), Aquacrop is more suitable for research on the response mechanism between yield and water (Ran et al., 2020) because it has a special irrigation management module that can set the irrigation method, amount of irrigation and related irrigation parameters. Another advantage of the AquaCrop model is that it requires fewer input parameters than most crop models while ensuring the requisite accuracy (Confalonieri et al., 2009). Many studies have shown that AquaCrop can

accurately simulate crop yield under different irrigation conditions (Abedinpour et al., 2012; Hellal et al., 2019; Ran et al., 2018, 2019, 2020).

According to the FAO's Irrigation and Drainage Paper no. 33 (Doorenbos and Kassam, 1979), the transfer equation of crop yield and water stress is shown as in Formula 1:

$$\frac{Y_x - Y_0}{Y_x} = k_y\left(\frac{ET_x - ET_0}{ET_x}\right) \quad (1)$$

where Y_x and Y_0 are the potential and the actual crop yields (kg/m^2), ET_x and ET_0 are the potential and actual evapotranspiration (mm), respectively, and k_y is the conversion coefficient between crop yield and water stress.

The model improves the equation by separating evapotranspiration (ET) into evaporation from soil (E) and crop transpiration (Tr) to avoid confusing between the effects of nonproductive and productive consumptive water. The final yield is expressed in terms of biomass (B) and the harvest index (HI), shown as Formulae 2 and 3, respectively:

$$Y = B \cdot HI \quad (2)$$

$$B = WP \cdot \sum Tr \quad (3)$$

where Y is final yield (kg/m^2), B is biomass (kg/m^2), HI is the harvest index, WP is the parameters of water productivity (kg/(m^2·mm)), and Tr is crop transpiration (mm).

The input data required by AquaCrop features four parts (Table 1): 1) meteorological data: These included daily precipitation from CN05.1, daily maximum and minimum temperature from ERA Interim, and the reference evapotranspiration calculated by the FAO's Penman-Monteith equation (Allen et al., 1998). 2) Soil data: These included the texture and organic content of soil obtained from WISE30sec, v1.0, to calculate such related parameters as permanent wilting coefficient, field capacity, saturated water content, and saturated conductivity. 3) Crop data: These mainly covered the parameters of growth and development (such as canopy coverage, root growth, and growth season), evaporation and transpiration, yield formation, and stress. The growth season was directly obtained from the Decade Dataset of Crop Growth and Development and Soil Moisture in China. The sensitive parameters were obtained from model calibration while non-sensitive parameters were obtained from the reference values of the crop model. In addition, the yield and sown area of maize were collected from 241 prefecture-level administrative regions. 4) Management data: These mainly included irrigation, fertilization, and surface coverage. The details of irrigation management are described below, and default values of the model were used for the other factors. The data mentioned above were acquired at different spatial resolutions. We unified their spatial resolutions to the prefecture-level administrative region before importing them to the AquaCrop model by following processing. For gridded meteorological data and soil data, we calculated the average value of all grids in each prefecture-level administrative region and took the average value as input. We obtained seasonal data on crop growth in each administrative region based on data collected at agricultural stations. For a given prefecture-level administrative region, if it had more than one station, we calculated the average of all stations in the region; if there was only one station, we used the seasonal crop growth data collected at it as input; if there was no station within the region, we used the value recorded at the nearest station as input.

2.3. Methods

2.3.1. Model calibration and validation

Model calibration is the basis of an accurate simulation. The aim here was to identify a set of genetic parameters for maize in different environments. Before calibration, it is necessary to select sensitive parameters that have the most significant effects on the results of the simulation because the many crop-related parameters of the AquaCrop model could not be calibrated one by one. The process of selecting sensitive parameters by analyzing the effects of changes in the input parameters on the results of the simulation is called sensitivity analysis, and can improve the efficiency of model calibration. We used the extended Fourier amplitude sensitivity test (EFAST) to select the sensitive parameters. EFAST is a method of global sensitivity analysis that emphasizes uncertainties in the entire parameter space, and considers the effects of the interactions among multiple parameters (Saltelli, 1999). The sensitivity index of each parameter was obtained by decomposing the results of variance in the simulation. The greater the sensitivity index is, the greater is the influence of the parameters on the results of the simulation. EFAST has been widely used in models of crop growth, such as the DSSAT (DeJonge et al., 2012), WOFOST (Wang et al., 2013b, 2013a), and AquaCrop (Vanuytrecht et al., 2014). In this study, we chose the two most sensitive parameters from 36 supported by the FAO.

We collected statistical data on maize yield in 241 prefecture-level administrative regions of China from 2002 to 2011. The yield data of the last two years were used for validation while the other data were used as samples for model calibration. By keeping the other parameters constant, we calibrated the two selected sensitive parameters region by region.

The steps of model calibration were as follows: 1) Set the range of the two sensitive parameters from 0.7 x to 1.3 x, where x is the reference value of the parameters supported by the FAO crop manual. 2) Search for the optimal parameter from 0.7 x to 1.3 x in increments of 0.02 x to modify the sensitive parameters and simulate the crop yield under various combinations. Use the normalized root mean square error (NRMSE) (Formula 4) as the standard to compare these simulated results with the statistical data under various combinations of the two parameters. Select the combination with the minimum NRMSE as the result of calibration for each prefecture-level administrative region:

$$\mathrm{NRMSE} = \frac{1}{\overline{O}}\sqrt{\frac{\sum_{i=1}^{n}(P_i - O_i)^2}{n}} \quad (4)$$

where n is the number of samples, O_i is the statistical yield of the ith sample, P_i is its simulated yield, and $\overline{O}$ is the average value of O_i.

Finally, we ran the calibrated model under actual meteorological and soil-related conditions for the validating years, and compared the simulated yield with the statistical yield to verify the accuracy of model calibration.

2.3.2. Irrigation scenario settings

The irrigation management function in AquaCrop was used to set scenarios of maize growth under different irrigation conditions. We setup two scenarios: 100% irrigation and rain-fed. Here, "100% irrigation" means that irrigation was immediately triggered once water shortage occurred, and water used for irrigation was equal to the demand. We then analyzed the scenarios where maize suffered from water stress in different stages of its growth. The crop's growth season was divided into four stages according to the definition in AquaCrop: the early growth stage, canopy growth stage, middle growth stage, and late growth stage, corresponding to periods from the sowing stage to the seventh leaf stage, the seventh leaf stage to the tasseling stage, the tasseling stage to the milk stage, and the milk stage to the physiological maturity of maize. For convenience, we simply number the four growth stages from 1 to 4, respectively. Drought might have occurred in any of the four growth stages, or in several successive or discontinuous stages at the same time. We simulated 14 irrigation scenarios in which irrigation occurred in stages 1, 2, 3, 4, stages 1 and 2, stages 1 and 3, stages 1 and 4, stages 2 and 3, stages 2 and 4, stages 3 and 4, stages 1, 2, and 3, stages 1, 2, and 4, stages 1, 3, and 4, and stages 2, 3, and 4. We ran the AquaCrop model under all the above scenarios. In addition to differences in irrigation, other model drivers including the meteorological conditions, nutrients

in soil, and field management settings were consistent such that the differences in the results were assumed to have been caused by water stress. As drought might have occurred in the growth stages with no irrigation, there were 14 possible scenarios of drought corresponding to the 14 irrigation scenarios.

2.3.3. Vulnerability curves

The Crop Water Stress Indicator (CWSI) was used to define the intensity of drought. It describes water stress by the extent to which actual evapotranspiration fails to meet potential evapotranspiration. The value ranges from zero to one: A larger CWSI represents higher water stress. The CWSI was affected by a series of factors, such as climate, properties of soil, and the genetic characteristics of the crop. The indicator can reflect the impact of drought on crop growth. It was calculated as follows:

$$\mathrm{CWSI} = 1 - \frac{ET}{ET_p} \tag{5}$$

where ET and ET_P respectively represents the actual and potential evapotranspiration (mm). Both were outputs of the AquaCrop model at a daily scale.

To reflect the cumulative effect of water stress, the drought hazard index (DHI) was defined as the daily average value of CWSI in the growth season (Formula 6):

$$\mathrm{DHI} = \frac{1}{n}\sum_{i=1}^{n}\mathrm{CWSI}_i \tag{6}$$

where DHI represents the drought hazard index, $\mathrm{CWSI_i}$ is the crop water stress index on the i^{th} day, and n is the number of days of the growth season. According to Wu et al. (2019), the drought level defined by the CWSI can be divided into four types: 0–0.25 as slight drought, 0.25–0.5 as moderate drought, 0.5–0.75 as severe drought, and 0.75–1 as extreme drought.

Based on the simulated yield obtained by the AquaCrop model, we defined the loss in yield caused by drought as the difference between the yields in the 100% irrigation scenario and the other scenarios. The yield loss rate (YLR) was calculated as follows:

$$\mathrm{YLR}(\%) = \left(1 - \frac{Y_2}{Y_1}\right) \cdot 100\% \tag{7}$$

where Y_1 and Y_2 respectively represent the maize yields (per unit) in the 100% irrigation scenario and the other scenarios, respectively.

Past research has shown that the logistic function can adequately describe the relationship between DHI and YLR (Jia et al., 2012; Wang et al., 2013b, 2013a; Yue et al., 2015; Cui et al., 2019). Therefore, we used the results of simulations of 37 years of the 241 regions as samples to construct the drought vulnerability curve by the logistic function.

2.3.4. Risk assessment

According to disaster system theory (Shi, 2002), the risk of drought is a function of the DHI, vulnerability, and exposure:

$$R = f(H, V, E) \tag{8}$$

where R, H, V, and E refer to risk, hazard, vulnerability, and exposure, respectively.

Without considering drought mitigation capacity, we set the exposure (E) of the regions that were maize growing to one. Then, risk was a function of hazard (H) and vulnerability (V). In this study, the hazard (H) of drought was assessed by the DHI based on a fixed probability of exceeding (5-, 10-, 20-, and 50-year return periods) (Chen et al., 2019; Wang et al., 2020c, 2020b). The DHIs for 1979–2015 were calculated based on output data from the AquaCrop simulation using Formula 6. The probability density function and cumulative distribution function of the DHI were formulated using the kernel density estimation method

Table 2
The 10 most sensitive parameters.

Parameter	Parameter description	Global sensitivity index	Ranking
Kcb	Crop coefficient when canopy growth is complete but prior to senescence	0.4271	1
HI0	Reference harvest index	0.2832	2
WP	Water productivity normalized for ET0 and CO2/g·m-2	0.2069	3
fshape-r	Shape factor describing root expansion	0.1334	4
WPy	Adjustment of water productivity in yield formation stage/%	0.1256	5
p-up3	Upper soil water depletion threshold for water stress effects on canopy senescence	0.1241	6
Zmin	Minimum effective rooting depth/m	0.1139	7
CCx	Maximum canopy cover	0.1100	8
GDDup	Minimum growing degree days required for full biomass production	0.1083	9
CGC	Canopy growth coefficient	0.0901	10

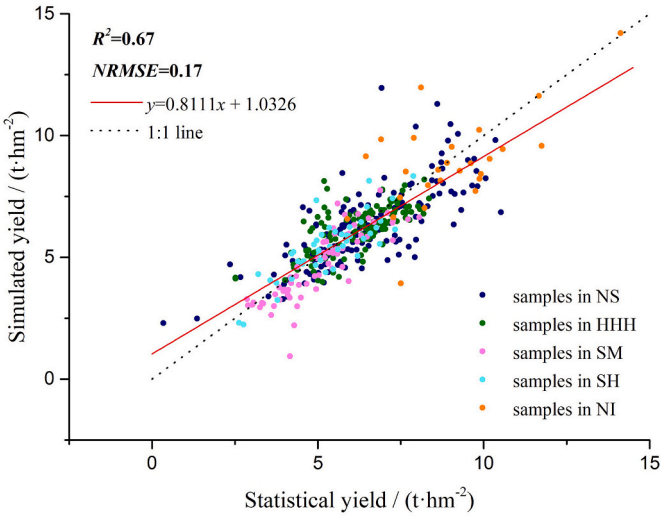

Fig. 2. Results of model validation.

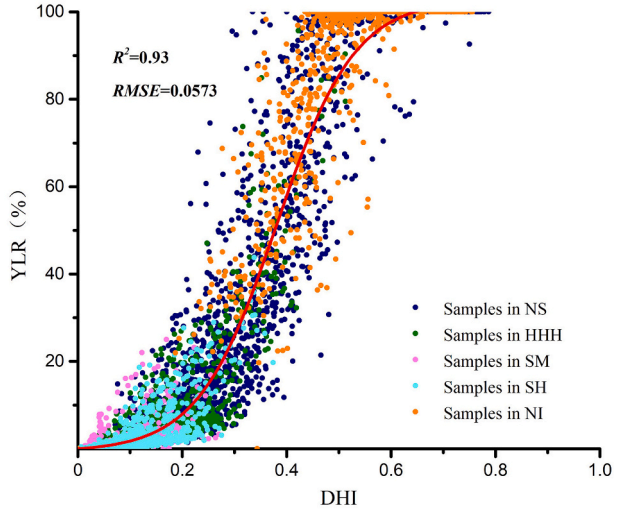

Fig. 3. Vulnerability curve for drought in the entire growth season of maize.

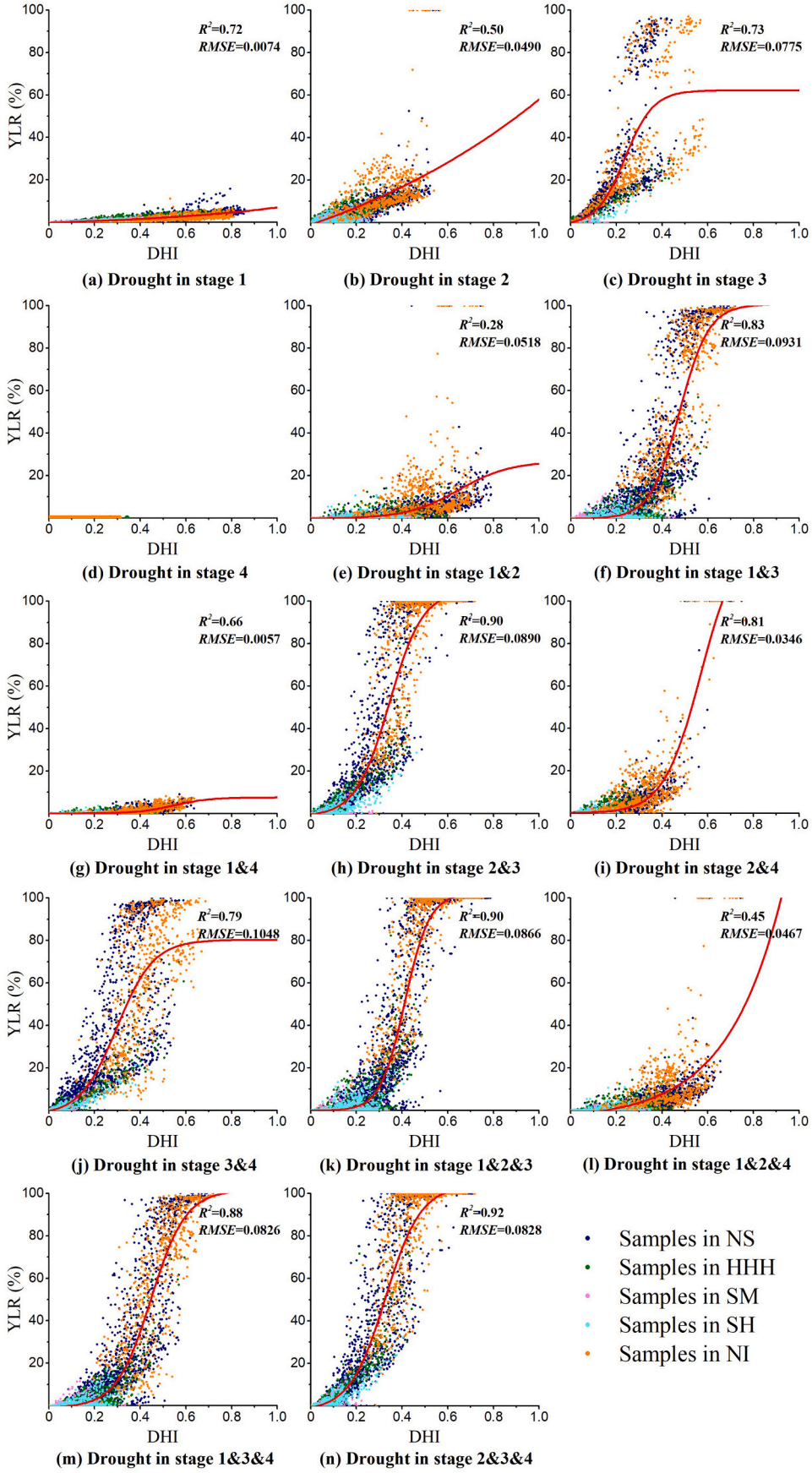

Fig. 4. Vulnerability curves for droughts in different growth stages.

(Silverman, 1986; Scott, 1992; Wand and Jones, 1995; Simonoff, 1996). We then calculated DHIs for 5-, 10-, 20-, and 50-year return periods. Finally, the vulnerability curve established in Section 2.3.3 was used to calculate the YLRs corresponding to the DHIs in different return periods, where this constituted the assessment of vulnerability.

3. Results

3.1. Model calibration and validation

The results of the global sensitivity analysis using EFAST are shown in Table 2. The two most sensitive parameters, K_{cb} and HI_0, were selected as ones to be calibrated.

Model calibration was conducted for each prefecture-level administrative region based on the yield data in 2002–2009. Therefore, we obtained 241 groups of values of K_{cb} and HI_0 corresponding to the 241 regions, ranging from 0.32– 1.79 and 0.14– 0.82, respectively. Based on the calibrated parameters, the maize yields in 2010 and 2011 were simulated and compared with the statistical maize yields to verify the accuracy of model calibration. The results are shown in Fig. 2. The Pearson's correlation coefficient of the simulated and statistical yields was 0.82 (significant at a level of 0.01). The slope of the regression equation was 0.81 so that the scatter points were concentrated near the 1:1 line. The coefficient of determination R^2 and NRMSE of the regression equation were 0.67 and 0.17, respectively. The simulated and actual statistical yields were similar, indicating that the model had been satisfactorily calibrated.

3.2. Vulnerability assessment

3.2.1. Vulnerability curve for the entire crop growth season

We used meteorological data from 1979 to 2015 to drive the calibrated AquaCrop model to simulate maize growth and yield under the different irrigation scenarios described in Section 3, and then used logistic functions to fit the drought vulnerability curves. Fig. 3 shows the vulnerability curves for the entire maize growth season. The function of the curve is as follows:

$$\mathrm{YLR}(\%) = \frac{103.6}{1 + 159.7e^{-13.34\times \mathrm{DHI}}} - 0.6329 \quad (9)$$

It generally followed an "S" shape. The scattered points in Fig. 3 were from the results of simulating five maize-growing regions in 1979–2015. The coefficient of determination R^2 was 0.93, indicating that the logistic curve could adequately describe the relationship between the DHI and the YLR. According to the curve, when the DHI was 0.2, the YLR began to increase significantly, while when the DHI was 0.6, the YLR was close to the maximum.

3.2.2. Vulnerability curves for various stages of crop growth

A total of 14 drought scenarios during different stages of maize growth were simulated. The fitting results of the drought vulnerability curves under these scenarios are shown in Fig. 4 and Table 3.

As for the entire growth season, the logistic function was used to describe the relationship between the DHI and the YLR. Values of R^2 of the 14 scenarios ranged from 0.28 to 0.92. For four scenarios in which drought occurred in single stages, the third stage had the greatest negative effect on maize yield, followed by the second, first, and the fourth stages, corresponding to periods from the tasseling stage to the milk stage, the seventh leaf stage to the tasseling stage, the sowing stage to the seventh leaf stage, and the milk stage to the physiological maturity stage, respectively. Of these four stages, the last was noteworthy: The YRL was always zero no matter how the DHI changed, indicating that the maize yield was no longer affected by water stress after the milk stage. For scenarios where drought occurred in more than one stage, the relationship between the DHI and the YLR became more complex but still conformed to the logistic function.

Table 3
Functions of the vulnerability curves with drought in various stages of growth.

Drought stage	Function	R^2	RMSE
1	$\mathrm{YLR}(\%) = \frac{1.713}{1 - 0.7895e^{0.12\times \mathrm{DHI}}} - 8.339$	0.72	0.0074
2	$\mathrm{YLR}(\%) = \frac{-9879}{1 + 0.0045e^{0.86\times \mathrm{DHI}}} + 9834$	0.50	0.0490
3	$\mathrm{YLR}(\%) = \frac{-63.57}{1 + 0.022e^{16.02\times \mathrm{DHI}}} + 62.22$	0.73	0.0775
4	/	/	/
1&2	$\mathrm{YLR}(\%) = \frac{-27.03}{1 + 0.0034e^{8.77\times \mathrm{DHI}}} + 26.75$	0.28	0.0518
1&3	$\mathrm{YLR}(\%) = \frac{101}{1 + 1679e^{-15.61\times \mathrm{DHI}}} - 0.3473$	0.83	0.0931
1&4	$\mathrm{YLR}(\%) = \frac{-7.542}{1 + 0.0009e^{12.83\times \mathrm{DHI}}} + 7.514$	0.66	0.0057
2&3	$\mathrm{YLR}(\%) = \frac{-106.6}{1 + 0.0092e^{13.64\times \mathrm{DHI}}} + 105.2$	0.90	0.0890
2&4	$\mathrm{YLR}(\%) = \frac{-129.7}{1 + 0.0008e^{12.48\times \mathrm{DHI}}} + 129.8$	0.81	0.0346
3&4	$\mathrm{YLR}(\%) = \frac{-82.6}{1 + 0.025e^{12.41\times \mathrm{DHI}}} + 80.27$	0.79	0.1048
1&2&3	$\mathrm{YLR}(\%) = \frac{-102.5}{1 + 0.0005e^{18.54\times \mathrm{DHI}}} + 102.3$	0.90	0.0866
1&2&4	$\mathrm{YLR}(\%) = \frac{103900}{1 + 45910e^{-4.16\times \mathrm{DHI}}} 4.26$	0.45	0.0467
1&3&4	$\mathrm{YLR}(\%) = \frac{-102.5}{1 + 0.0028e^{13.15\times \mathrm{DHI}}} + 101.5$	0.88	0.0826
2&3&4	$\mathrm{YLR}(\%) = \frac{-106.2}{1 + 0.015e^{12.86\times \mathrm{DHI}}} + 103.9$	0.92	0.0828

3.3. Risk assessment

3.3.1. Drought Hazard Index based on fixed probability of exceeding

The distributions of the DHI at the four risk levels (5-, 10-, 20-, and 50-year return periods) were calculated on the basis of the 37-year simulation (1979–2015), as shown in Fig. 5. The results showed that drought in China decreased from northwest to southeast. Table 4 shows the average DHI of the five maize-growing regions under different levels of risk. According to them, the Northwest Irrigated Maize Region (NI) had the largest drought hazard, and its DHIs at all four risk levels were higher than 0.5 (0.5397– 0.5994), indicating that the region's drought intensity was the most significant. This was followed by the North Spring Maize Region (NS), with an average DHI between 0.3023 and 0.3851, the Huang-Huai-Hai Summer Maize Region (HHH), with an average DHI between 0.1741 and 0.2488, the South Hilly Maize Region (SH), with an average DHI between 0.1378 and 0.2032, and the Southwest Mountain Maize Region (SM), with an average DHI between 0.0896 and 0.141.

3.3.2. Risk of yield loss

Based on the distribution of the DHI and the equations for vulnerability regression, the distributions of the risk of yield loss under the corresponding risk levels (return periods of 5, 10, 20, and 50 years) was obtained (Fig. 6). In accordance with the trend of DHI distribution, the risk of yield loss in China was also found to be decreasing from northwest to southeast. The average YLR values of the five maize-growing regions in the order from large to small were: the Northwest Irrigated Maize Region (NI), with an average YRL between 86.17% and 93.39%, the North Spring Maize Region (NS), with an average YRL between 31.69% and 46.2%, the Huang-Huai-Hai Summer Maize Region (HHH), with an average YRL between 7.73% and 18.35%, the South Hilly Maize Region (SH), with an average YRL between 4.26% and 11.08%, and the Southwest Mountain Maize Region (SM), with an average YRL between 1.58% and 4.25% (Table 5). The results showed that maize production in northwest China was almost completely reliant on irrigation, whereas in the south and southwest, natural precipitation met most of the demand of maize for water.

4. Discussion

In previous vulnerability studies, the accumulative value of the daily crop water stress index has been used to describe the DHI (this method

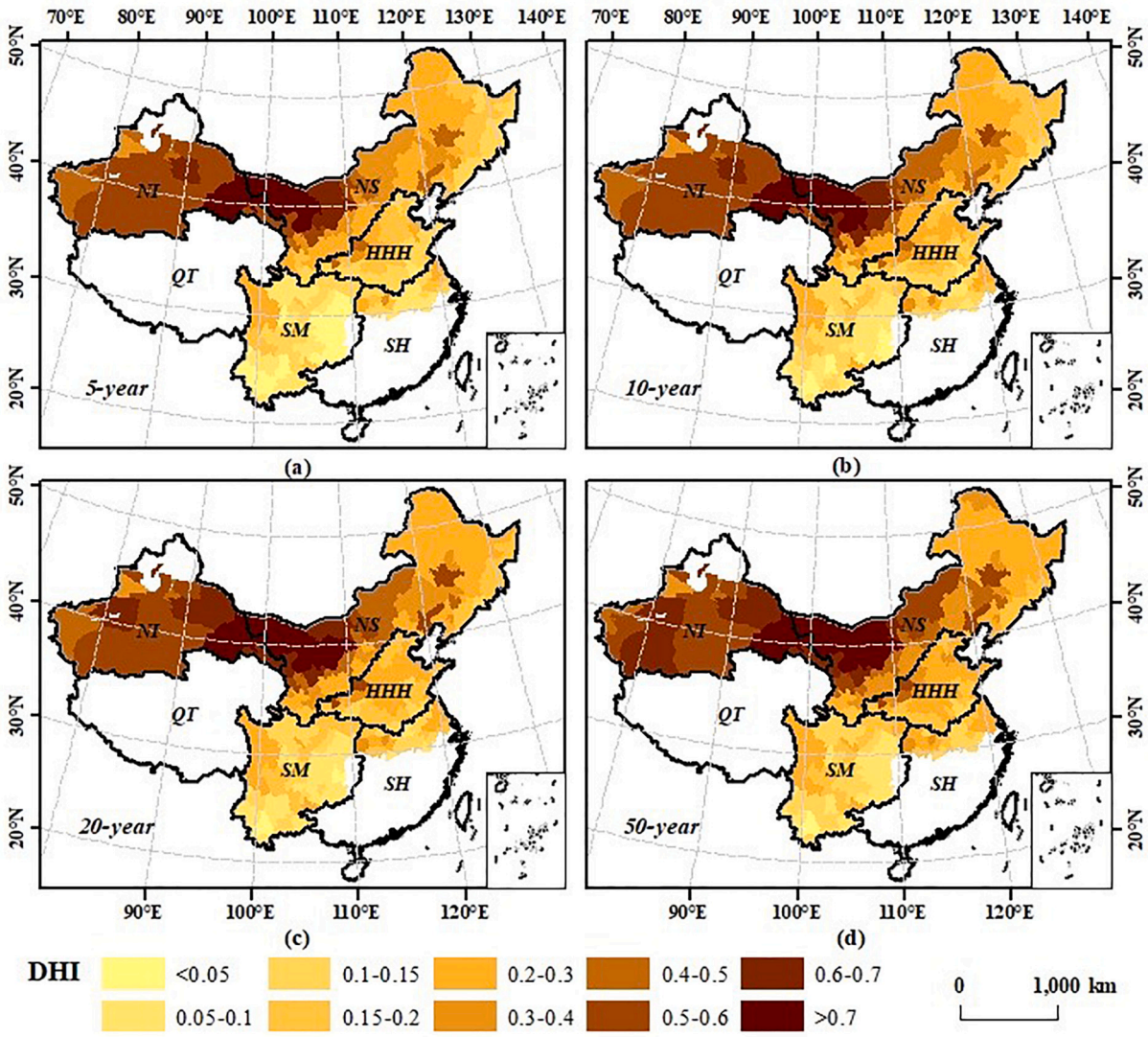

Fig. 5. Drought hazard indices of 241 prefecture-level administrative regions in China based on a fixed exceeding probability: (a) 5-year return period, (b) 10-year return period, (c) 20-year return period, and (d) 50-year return period.

referred to hereinafter as the "accumulative method") (Yin et al., 2014; Guo et al., 2016; Wang et al., 2010; Yue et al., 2015; Jia et al., 2016). This paper proposed a method on this basis by using the daily average value of the crop water stress index instead of the traditional accumulative value to construct the DHI (the proposed method is referred to hereinafter as the "average method").

The traditional accumulative method is as follows:

$$DHI_k = \frac{\sum_{i=1}^{n} CWSI_i}{max(DHI_k)} \quad (10)$$

where DHI_k represents the DHI in the k^{th} prefecture-level administrative region, $CWSI_i$ represents the crop water stress index on the i^{th} day, and n is the number of days of the growth season.

The accumulative method considered the accumulative effect of droughts but has some disadvantages. When the growth period of crops ended ahead of schedule owing to severe water stress, the DHI calculated by the accumulative method was smaller than the actual value. In this situation, some outliers that had a small DHI but high yield loss rate might have been obtained, where this led to a deviation in the fitting results of the vulnerability curves. Moreover, the accumulative DHI might have been greater than one. The DHI calculated by accumulative method was then adjusted in the range 0–1 by standardization, which hindered a comparison of the intensities of water stress among regions because the ranges of the original DHIs of different regions were different.

Table 4
Average drought hazard indices of five maize-growing regions in different return periods.

Region	Return period			
	5-year	10-year	20-year	50-year
NS	0.3023	0.3320	0.3556	0.3851
HHH	0.1741	0.1983	0.2201	0.2488
SM	0.0896	0.1089	0.1248	0.1410
SH	0.1378	0.1647	0.1835	0.2032
NI	0.5397	0.5614	0.5795	0.5994

To solve the above problems, we proposed the "average method" to calculate the DHI instead of the accumulative method. The calculation is shown in Formula 5, and involves dividing the accumulative DHI by the number of days of the growth season. Therefore, when the crop had grown for the entire season, the intensities of drought described by the two methods showed no difference. But in the case where crop growth

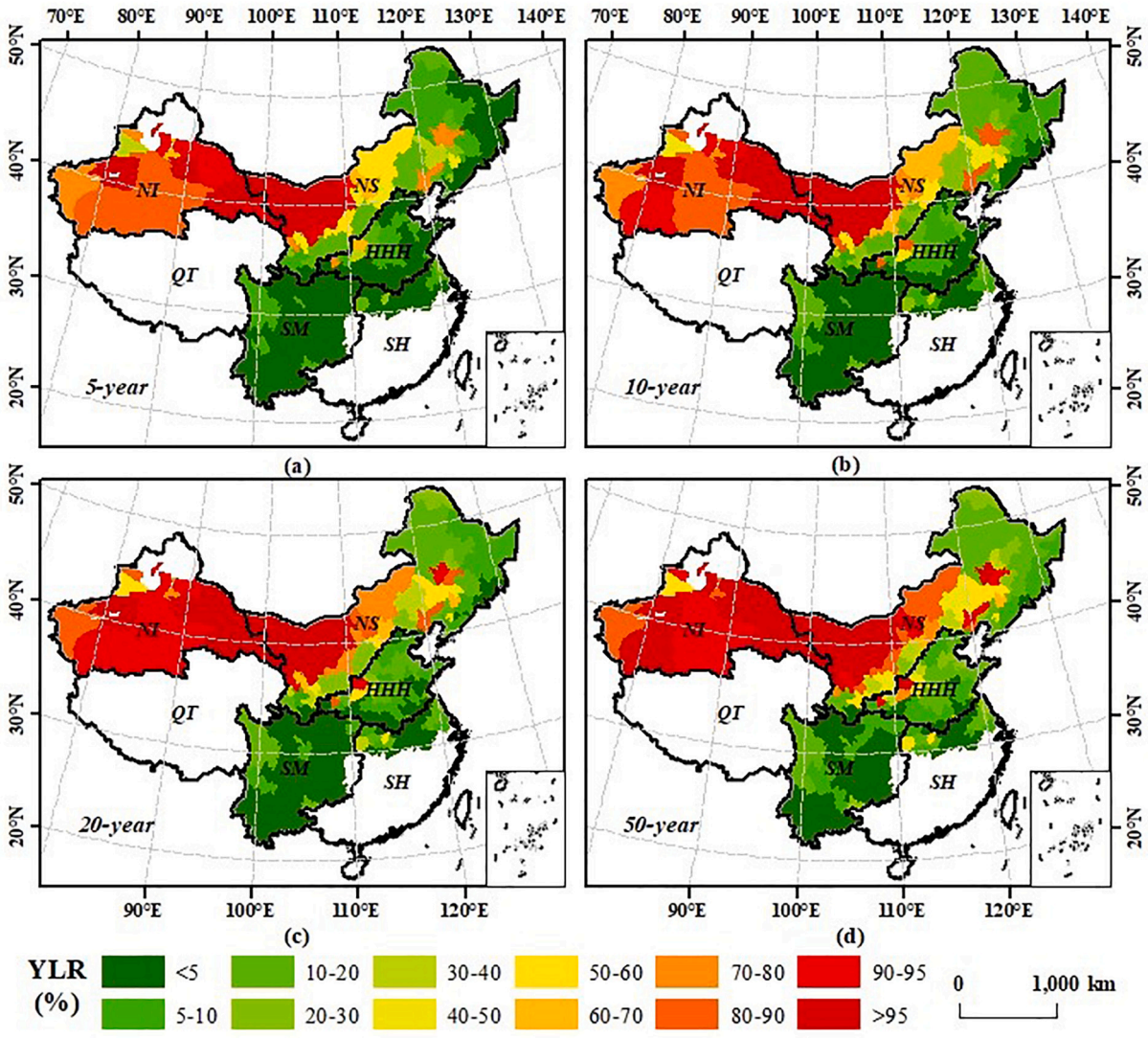

Fig. 6. Yield loss rate of 241 prefecture-level administrative regions in China based on fixed exceeding probabilities: (a) 5-year return period, (b) 10-year return period, (c) 20-year return period, and (d) 50-year return period.

Table 5
Average yield loss risks of five maize-growing regions in different return periods.

Region	5-year	10-year	20-year	50-year
NS	31.69%	36.54%	40.65%	46.20%
HHH	7.73%	10.37%	13.22%	18.35%
SM	1.58%	2.40%	3.23%	4.25%
SH	4.26%	6.58%	8.60%	11.08%
NI	86.17%	89.24%	91.39%	93.39%

season ended ahead of schedule, using the average method helped avoid the problems mentioned above. The range of values of the CWSI was between zero and one, and the DHI calculated by the "average method" did not require standardization. It was able to preserve its physical meaning as the CWSI, and could be easily used to compare the intensities of water stress between regions.

To verify the above, we used both methods to construct the DHI in the five maize-growing regions (Fig. 7). The results showed that in regions with higher drought intensities, such as the Northwest Irrigated Maize Region (NI), North Spring Maize Region (NS), and the Huang-Huai-Hai Summer Maize Region (HHH), for sample points with yield loss rates close to one, the DHIs calculated by the cumulative method were significantly smaller than those calculated by the average method, which was consistent with theoretical expectation. Furthermore, the results of two methods also exhibited differences in the Southwest Mountain Maize Region (SM) and the South Hilly Maize Region (SH) due to deviations caused by standardization in the accumulative method.

Research on the vulnerability of crops to drought has shown that the risk of yield loss grows non-linearly with an increase in drought severity (Leng and Hall, 2019). Cui et al. (2019) and Wei et al. (2019) divided the vulnerability curve into three parts using two inflection points called the "disaster-inducing point" and the "disaster-ceasing point". The three parts were the "initial phase", "developing phase" and "declining phase". In our study, the drought vulnerability curve showed that the rate of increase of YLR was slow when the DHI was under 0.2, increased when the DHI was between 0.2 and 0.6, and finally became slow again when the DHI was above 0.6. Referring to past work (Cui et al., 2019; Wei et al., 2019), DHI = 0.2 was the disaster-inducing point where the drought grade started to develop from slight to moderate, and YLR grew the most quickly. The vulnerability curve changed from the initial phase to the developing phase, because of which the YLR began to increase significantly. DHI = 0.6 was the disaster-ceasing point, where the drought became severe and the YLR decreased most rapidly. The curve entered the declining phase, and the influence of drought on maize growth and yield was close to the upper limit for guaranteeing the survival of the plants. When the water stress increased, the plants died

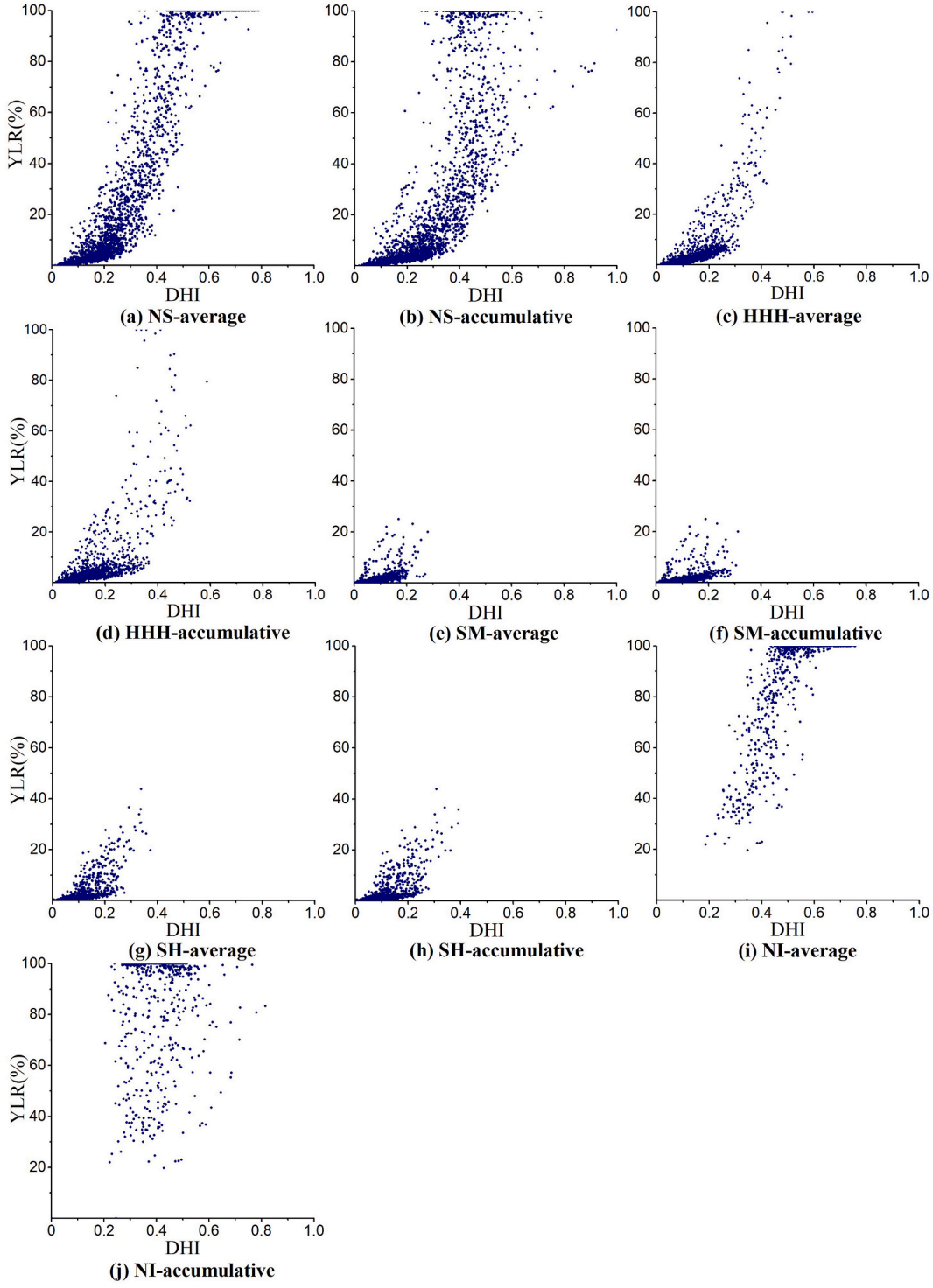

Fig. 7. Comparisons of the average and the accumulative methods in the five maize-growing regions.

from a lack of water. The corresponding crop yield loss might thus have been close to 100%.

Combined with the results in Section 3.3, we see that although the risk of drought in the North Spring Maize Region and the Huang-Huai-Hai Summer Maize Region was significantly lower than that in the Northwest Irrigated Maize Region, the DHI values of these two regions mostly fell in the "developing phase," indicating the most sensitive response of crop yield to water stress. Therefore, the efficiency of irrigation of these two regions was theoretically the highest because the same amount of water could significantly reduce the loss of crop yield. Moreover, the North Spring Maize Region and the Huang-Huai-Hai Summer Maize Region had the largest maize production in China. Thus, the local government should clarify the demands for agricultural irrigation and regulate water resources appropriately to meet agricultural demand. In addition, agricultural water-saving irrigation technology should be developed and the efficiency of utilization of water should be improved. The risk of drought in the Northwest Irrigated Maize Region was the most serious, and the average risk of yield loss was 86.17% ~ 93.39%. The region's agricultural production depended almost entirely on irrigation. In these extremely arid areas, the

government needs to guide the adjustment of agricultural planting and the development of drought-resistant varieties of crops. Finally, the Southwest Mountain Maize Region and the South Hilly Maize Region had enough natural precipitation to meet the needs of crop growth, and agricultural production was less dependent on irrigation. Although the risk of drought events in these regions was low, farmers should take the relevant emergency measures to prevent the occurrence of sudden drought events.

We identified the drought-sensitive period of maize growth by analyzing its vulnerability to drought in various stages of growth, and clarified its mechanism of water demand and consumption to some extent. It has been shown that more than 75% of the field capacity of maize was needed during the sowing and emergence stages, 70% ~ 75% in the jointing stage, nearly 100% in the tasseling stage, and 65% at the end of the milk stage (Chen and Guo, 1995). The tasseling stage was the most important stage for yield accumulation. Our research also showed that the negative effects of drought in the tasseling stage was the most serious. These results can provide a theoretical basis for the prevention of yield loss due to drought.

Due to limitations related to the availability of data, some uncertainties were obtained in our research. For example, in inputs to the AquaCrop model, because of a lack of field management data (fertilization, pesticides, and surface practices), we had to use the model's default values. We also made some assumptions regarding the uniformity of the spatial distribution of maize planting and ignored differences between different varieties of maize. All these might have led to deviations between the results of our simulation and the actual situation. A more detailed distinction is needed between varieties of crops and their corresponding planting proportions in the future research to overcome these limitations.

5. Conclusions

This paper proposed a method of the vulnerability and risk assessments of drought for maize crops based on the AquaCrop model. The main results are as follows:

1) The drought vulnerability curve of maize for the entire growth season followed an "S" shape, the coefficient of determination R^2 was 0.93, indicating that the relationship between the DHI and the YLR was in accordance with the logistic function. The results showed that when the DHI approached 0.2, the YLR began to increase significantly, and when the DHI reached 0.6, the YLR was close to its maximum value.
2) For various growth stages, the values of R^2 of 14 scenarios ranged from 0.28 to 0.92. For four scenarios where drought occurred in a single stage, drought in periods from the tasseling stage to the milk stage had the largest negative effect on maize yield, followed by the seventh leaf stage to the tasseling stage, the sowing stage to the seventh leaf stage, and the milk stage to the physiological maturity stage. Maize yield was no longer affected by water stress once in the milk stage. The relationship between the DHI and the YLR became more complex when drought occurred in more than one stage.
3) Under all four risk levels (return periods of 5, 10, 20, and 50 years), the DHI and YRL of maize in China exhibited a trend of decrease from northwest to southeast. The average DHIs and YLRs of the five maize-growing regions in the order from large to small were: the Northwest Irrigated Maize Region (DHI: 0.5397– 0.5994; YLR: 86.17% ~ 93.39%), the North Spring Maize Region (DHI: 0.3023– 0.3851; YLR: 31.69% ~ 46.2%), the Huang-Huai-Hai Summer Maize Region (DHI: 0.1741– 0.2488; YLR: 7.73% ~ 18.35%), the South Hilly Maize Region (DHI: 0.1378– 0.2032; YLR: 4.26% ~ 11.08%), and the Southwest Mountain Maize Region (DHI: 0.0896– 0.141; YLR: 1.58% ~ 4.25%).
4) It is better to using the daily average value of the crop water stress index than the traditional accumulative value to construct the DHI. The average method solves the problem whereby the DHI calculated by the accumulative method is smaller than its actual value when the growth period of crops ends ahead of schedule owing to severe water stress. Moreover, it then becomes easier to compare the intensities of water stress among regions.

Declaration of Competing Interest

None.

Acknowledgments

This work was supported by the National Key R&D Program of China (Grant No. 2019YFA0606900), and the National Natural Science Foundation of China (Grant No. 42077436).

References

Abedinpour, M., Sarangi, A., Rajput, T.B.S., Singh, M., Pathak, H., Ahmad, T., 2012. Performance evaluation of AquaCrop model for maize crop in a semi-arid environment. Agric. Water Manag. 110, 55–66.
Aherne, J., Larssen, T., Cosby, B.J., Dillon, P.J., 2006. Climate variability and forecasting surface water recovery from acidification: modelling drought-induced sulphate release from wetlands. Sci. Total Environ. 365 (1–3), 186–199.
Ahmadalipour, A., Moradkhani, H., Castelletti, A., Magliocca, N., 2019. Future drought risk in Africa: integrating vulnerability, climate change, and population growth. Sci. Total Environ. 662, 672–686.
Allen, R., Pereira, L.S., Raes, D., Smith, M., 1998. Crop Evapotranspiration–Guidelines for Computing Crop Water Requirements. In: FAO Irrigation and Drainage Paper N° 56. Rome, Italy.
Bell, R., Glade, T., 2004. Quantitative risk analysis for landslides - examples from Bildudalur, NW-Iceland. Nat. Hazards Earth Syst. Sci. 4 (1), 117–131.
Birkmann, J., 2006. Measuring Vulnerability to Promote Disaster-Resilient Societies: Conceptual Frameworks and Definitions. In: Measuring Vulnerability to Natural Hazards: Towards Disaster Resilient Societies. United Nations University Press, Tokyo.
Burke, E.J., Brown, S.J., Christidis, N., 2006. Modeling the recent evolution of global drought and projections for the twenty-first century with the Hadley Centre climate model. J. Hydrometeorol. 7 (5), 1113–1125.
Cappabianca, F., Barbolini, M., Natale, L., 2008. Snow avalanche risk assessment and mapping: a new method based on a combination of statistical analysis, avalanche dynamics simulation and empirically-based vulnerability relations integrated in a GIS platform. Cold Reg. Sci. Technol. 54 (3), 193–205.
Carrao, H., Naumann, G., Barbosa, P., 2016. Mapping global patterns of drought risk: An empirical framework based on sub-national estimates of hazard, exposure and vulnerability. Global Environmental Change-Human and Policy Dimensions 39, 108–124.
Chen, F., Jia, H., Pan, D., 2019. Risk assessment of maize drought in China based on physical vulnerability. J. Food Qual. 2019, 1–9.
Chen, Y., Guo, G., 1995. Main Crop Water Requirement and Irrigation of China. China Water and Power Press, Beijing (in Chinese).
Cheng, L., Hoerling, M., AghaKouchak, A., Livneh, B., Quan, X., Eischeid, J., 2016. How has human-induced climate change affected California drought risk? J. Clim. 29 (1), 111–120.
Chou, J., Xian, T., Zhao, R., Xu, Y., Yang, F., Sun, M., 2019. Drought risk assessment and estimation in vulnerable eco-regions of China: under the background of climate change. Sustainability 11 (16), 4463.
Colombi, M., Borzi, B., Crowley, H., Onida, M., Meroni, F., Rui, P., 2008. Deriving vulnerability curves using Italian earthquake damage data. Bull. Earthq. Eng. 6 (3), 485–504.
Confalonieri, R., Acutis, M., Bellocchi, G., Donatelli, M., 2009. Multi-metric evaluation of the models WARM, CropSyst, and WOFOST for rice. Ecol. Model. 220 (11), 1395–1410.
Cui, Y., Jiang, S., Jin, J., Ning, S., Feng, P., 2019. Quantitative assessment of soybean drought loss sensitivity at different growth stages based on S-shaped damage curve. Agric. Water Manag. 213, 821–832.
Dai, A., 2013. Increasing drought under global warming in observations and models. Nat. Clim. Chang. 3 (2), 52–58.
Dai, A., Zhao, T., Chen, J., 2018. Climate change and drought: a precipitation and evaporation perspective. Curr. Climate Change Rep. 4, 301–312.
DeJonge, K.C., Ascough II, J.C., Ahmadi, M., Andales, A.A., Arabi, M., 2012. Global sensitivity and uncertainty analysis of a dynamic agroecosystem model under different irrigation treatments. Ecol. Model. 231, 113–125.
Diepen, C.A., Wolf, J., Keulen, H., Rappoldt, C., 1989. WOFOST: a simulation model of crop production. Soil Use Manag. 5 (1), 16–24.
Dilley, M., 2005. Natural disaster hotspots: a global risk analysis. Uwe Deichmann 20 (4), 1–145.
Doorenbos, J., Kassam, A.H., 1979. Yield Response to Water. In: Irrigation and Drainage Paper N. 33. FAO, Rome, Italy.
Dutta, D., Herath, S., Musiakec, K., 2003. A mathematical model for flood loss estimation. J. Hydrol. 277 (1–2), 24–49.

FAO. (2013). UN lays foundations for more drought resilient societies. Retrieved from: http://fao.org/news/story/en/item/172030/icode/.
FAO, 2017. Global report on food crises 2017. Retrieved from: http://www.fao.org/fileadmin/user_upload/newsroom/docs/20170328_Full%20Report_Global%20Report%20on%20Food%20Crises_v1.pdf.
Feng, P., Liu, D., Wang, B., Waters, C., Zhang, M., Yu, Q., 2019. Projected changes in drought across the wheat belt of southeastern Australia using a downscaled climate ensemble. Int. J. Climatol. 39 (2), 1041–1053.
Foster, T., Brozovic, N., Butler, A.P., Neale, C.M.U., Raes, D., Steduto, P., Fereres, E., Hsiao, T.C., 2017. AquaCrop-OS: An open source version of FAO's crop water productivity model. Agric. Water Manag. 181, 18–22.
Galli, M., Guzzetti, F., 2007. Landslide vulnerability criteria: a case study from Umbria, Central Italy. Environ. Manag. 40 (4), 649–664.
Gizaw, M.S., Gan, T.Y., 2017. Impact of climate change and El Nio episodes on droughts in sub-Saharan Africa. Clim. Dyn. 49 (1–2), 665–682.
Guo, H., Zhang, X., Lian, F., Gao, Y., Lin, D., Wang, J., 2016. Drought risk assessment based on vulnerability surfaces: a case study of maize. Sustainability 8 (8), 813.
Hanson, P.J., Weltzin, J.F., 2000. Drought disturbance from climate change: response of United States forests. Sci. Total Environ. 262 (3), 205–220.
Hellal, F., Mansour, H., Abdel-Hady, M., El-Sayed, S., Abdelly, C., 2019. Assessment water productivity of barley varieties under water stress by AquaCrop model. Aims Agriculture and Food 4 (3), 501–517.
Hohl, R., Schiesser, H.H., Aller, D., 2002. Hailfall: the relationship between radar-derived hail kinetic energy and hail damage to buildings. Atmos. Res. 63 (3–4), 177–207.
IPCC, 2014. Climate Change 2014: Impact, Adaption, and Vulnerability. Cambridge University Press, Cambridge. Retrieved from: https://www.ipcc.ch/report/ar5/wg2/.
Jia, H., Wang, J., Cao, C., Pan, D., Shi, P., 2012. Maize drought disaster risk assessment of China based on EPIC model. Int. J. Digital Earth 5 (6), 488–515.
Jia, H., Pan, D., Li, J., Zhang, W., Rasul, G., 2016. Risk assessment of maize drought disaster in Southwest China using the environmental policy integrated climate model. J. Mt. Sci. 13 (3), 465–475.
Jones, J.W., Hoogenboom, G., Porter, C.H., Boote, K.J., Batchelor, W.D., Hunt, L.A., Wilkens, P.W., Singh, U., Gijsman, A.J., Ritchie, J.T., 2003. The DSSAT cropping system model. Eur. J. Agron. 18 (3–4), 235–265.
Keylock, C.J., Barbolini, M., 2001. Snow avalanche impact pressure - vulnerability relations for use in risk assessment. Can. Geotech. J. 38 (2), 227–238.
Khajwal, A., Noshadravan, A., 2020. Probabilistic hurricane wind-induced loss model for risk assessment on a regional scale. ASCE-ASME Journal of Risk and Uncertainty in Engineering Systems Part A-Civil Engineering 6 (2), 04020020.
Khanduri, A.C., Morrow, G.C., 2003. Vulnerability of buildings to windstorms and insurance loss estimation. J. Wind Eng. Ind. Aerodyn. 91 (4), 455–467.
Kurniasih, E., Impron, Perdinan. (2017). Use of drought index and crop modelling for drought impacts analysis on maize (*Zea mays* L.) yield loss in Bandung District. *Iop Conference Series: Earth and Environmental Science*, 58: 012036.
Lee, K.H., Rosowsky, D.V., 2005. Fragility assessment for roof sheathing failure in high wind regions. Eng. Struct. 27 (6), 857–868.
Leng, G., Hall, J., 2019. Crop yield sensitivity of global major agriculture countries to droughts and the projected changes in the future. Sci. Total Environ. 654, 811–821.
Lesk, C., Rowhani, P., Ramankutty, N., 2016. Influence of extreme weather disasters on global crop production. Nature 529 (7584), 84–87.
Linares, R., Roque, C., Gutierrez, F., Zarroca, M., Carbonel, D., Bach, J., Fabregat, I., 2017. The impact of droughts and climate change on sinkhole occurrence. A case study from the evaporite karst of the Fluvia Valley, NE Spain. Sci. Total Environ. 579, 345–358.
Mao, Y., Wu, Z., He, H., Lu, G., Xu, H., Lin, Q., 2017. Spatio-temporal analysis of drought in a typical plain region based on the soil moisture anomaly percentage index. Sci. Total Environ. 576, 752–765.
Orsini, G., 2012. A model for buildings' vulnerability assessment using the parameter less scale of seismic intensity (PSI). Earthquake Spectra 15 (3), 463–483.
Ran, H., Kang, S., Ki, F., Du, T., Tong, L., Li, S., Ding, R., Zhang, X., 2018. Parameterization of the AquaCrop model for full and deficit irrigated maize for seed production in arid Northwest China. Agric. Water Manag. 203, 438–450.
Ran, H., Kang, S., Hu, X., Li, F., Du, T., Tong, L., Li, S., Ding, R., Zhou, Z., David, P., 2019. Newly developed water productivity and harvest index models for maize in an arid region. Field Crop Res. 234, 73–86.
Ran, H., Kang, S., Hu, X., Li, S., Wang, W., Liu, F., 2020. Capability of a solar energy-driven crop model for simulating water consumption and yield of maize and its comparison with a water-driven crop model. Agric. For. Meteorol. 287, 107955.
Ranjbar, P.R., Naderpour, H., 2020. Probabilistic evaluation of seismic resilience for typical vital buildings in terms of vulnerability curves. Structures 23, 314–323.
Rosenzweig, C., Elliott, J., Deryng, D., Ruane, A.C., Mueller, C., Arneth, A., Boote, K.J., Folberth, C., Glotter, M., Khabarov, N., Neumann, K., Piontek, F., Pugh, T.A.M., Schmid, E., Stehfest, E., Yang, H., Jones, J.W., 2014. Assessing agricultural risks of climate change in the 21st century in a global gridded crop model intercomparison. Proc. Natl. Acad. Sci. U. S. A. 111 (9), 3268–3273.
Saltelli, A., 1999. Sensitivity analysis: could better methods be used? J. Geophys. Res.-Atmos. 104 (D3), 3789–3793.
Scott, D.W., 1992. Multivariate Density Estimation. In: Theory, Practice and Visualization. Wiley, New York.
Shan, D., Qu, F., Deng, X., 2020. Seismic fragility analysis of irregular bridges with non-circular tall piers considering ground motion directionality. Bull. Earthq. Eng. 18 (4), 1723–1753.
Shi, H., Chen, J., Wang, K., Niu, J., 2018. A new method and a new index for identifying socioeconomic drought events under climate change: a case study of the East River basin in China. Sci. Total Environ. 616, 363–375.
Shi, P.J., 2002. Theory and practice on disaster system research in a third time. Journal of Natural Disasters 11 (3), 1–9 (in Chinese with Englishi abstract).
Shi, P.J., 2011. Atlas of Natural Disaster Risk of China. Science Press, Beijing.
Silverman, B.W., 1986. Density Estimation for Statistics and Data Analysis. Chapman and Hall, London.
Simonoff, J.S., 1996. Smoothing Method in Statistics. Springer, New York.
Singhal, A., Kiremidjian, A.S., 1996. Method for probabilistic evaluation of seismic structural damage. J. Struct. Eng. 122 (12), 1459–1467.
Smith, D.I. (1994). Flood damage estimation - a review of urban stage-damage curves and loss functions. *Water S. A*, 20(3): 231–238.
Steduto, P., 2003. Biomass water-productivity comparing the growth-engines of crop models. FAO Expert Consultation on Crop Water Productivity Under Deficient Water Supply 26–28.
Steduto, P., Hsiao, T.C., Raes, D., Fereres, E., 2009. AquaCrop—the FAO crop model to simulate yield response to water: I. concepts and underlying principles. Agron. J. 101 (3), 426–437.
Tietjen, B., Schlaepfer, D.R., Bradford, J.B., Lauenroth, W.K., Hall, S.A., Duniway, M.C., Hochstrasser, T., Jia, G., Munson, S.M., Pyke, D.A., Wilson, S.D., 2017. Climate change-induced vegetation shifts lead to more ecological droughts despite projected rainfall increases in many global temperate drylands. Glob. Chang. Biol. 23 (7), 2743–2754.
Todorovic, M., Albrizio, R., Zivotic, L., Saab, M.T.A., Stockle, C., Steduto, P., 2009. Assessment of AquaCrop, CropSyst, and WOFOST models in the simulation of sunflower growth under different water regimens. Agron. J. 101 (3), 509–521.
Tong, P., 1992. Regionalization of Maize Growing Areas in China. China Agricultural Science and Technology Press, Beijing (in Chinese).
UNISDR. (2009). Terminology on Disaster Risk Reduction. Retrieved from: https://www.unisdr.org/we/inform/terminology.
Vanuytrecht, E., Raes, D., Willems, P., 2014. Global sensitivity analysis of yield output from the water productivity model. Environ. Model. Softw. 51, 323–332.
Wand, M.P., Jones, M.C., 1995. Kernel Smoothing. Chapman and Hall, London.
Wang, B., Feng, P., Liu, D., Waters, C., 2020a. Modelling biophysical vulnerability of wheat to future climate change: a case study in the eastern Australian wheat belt. Ecol. Indic. 114, 106290.
Wang, J., Li, X., Lu, L., Fang, F., 2013b. Parameter sensitivity analysis of crop growth models based on the extended Fourier amplitude sensitivity test method. Environ. Model. Softw. 48, 171–182.
Wang, Q., Wu, J., Li, X., Zhou, H., Yang, J., Geng, G., An, X., Liu, L., Tang, Z., 2017. A comprehensively quantitative method of evaluating the impact of drought on crop yield using daily multi-scale SPEI and crop growth process model. Int. J. Biometeorol. 61 (4), 685–699.
Wang, R., Zhang, J., Guo, E., Alu, S., Li, D., Ha, S., Dong, Z., 2019. Integrated drought risk assessment of multi-hazard-affected bodies based on copulas in the Taoerhe Basin, China. Theor. Appl. Climatol. 135 (1–2), 577–592.
Wang, W., Wu, F., Wang, Z., 2020c. Revising seismic vulnerability of bridges based on Bayesian updating method to evaluate traffic capacity of bridges. Sustainability 12 (5), 1898.
Wang, Y., Lv, J., Wang, Y., Sun, H., Hannaford, J., Su, Z., Barker, L., & Qu., Y. (2020b). Drought risk assessment of spring maize based on APSIM crop model in Liaoning province, China. Int. J. Disaster Risk Reduc., 45: 101483.
Wang, Z., Fang, W., Shi, P., Fei, H., Hong, X., 2010. Assessment on typical drought risk for wheat production in China based on natural vulnerability. Arid Zone Research 27 (1), 23–35.
Wang, Z., He, F., Fang, W., Liao, Y., 2013a. Assessment of physical vulnerability to agricultural drought in China. Nat. Hazards 67 (2), 645–657.
Wei, Y., Jin, J., Jiang, S., Ning, S., Cui, Y., Zhou, Y., 2019. Simulated assessment of summer maize drought loss sensitivity in Huaibei plain, China. Agronomy Basel 9 (2), 78.
Wilhite, D.A., 2000. Drought as a natural Hazard: Concepts and definitions. In: Wilhite, D.A. (Ed.), Drought: A Global Assessment. Routledge Publishers, London, pp. 3–18.
Wisner, B., 2004. At Risk: Natural Hazards, People's Vulnerability and Disasters. Psychology Press, London.
Wu, H., Wilhite, D.A., 2004. An operational agricultural drought risk assessment model for Nebraska, USA. Nat. Hazards 33 (1), 1–21.
Wu, H., Xiong, D., Liu, B., Zhang, S., Yuan, Y., Fang, Y., Chidi, C., Dahal, N., 2019. Spatio-temporal analysis of drought variability using CWSI in the Koshi River basin (KRB). Int. J. Environ. Res. Public Health 16 (17).
Wu, Z., Shen, Y., Wang, H., Wu, M., 2020. Quantitative assessment of urban flood disaster vulnerability based on text data: case study in Zhengzhou. Water Sci. Technol. Water Supply 20 (2), 408–415.
Xie, W., Xiong, W., Pan, J., Ali, T., Cui, Q., Guan, D., Meng, J., Mueller, N.D., Lin, E., Davis, S.J., 2018. Decreases in global beer supply due to extreme drought and heat. Nature Plants 4 (11), 964–973.
Yang, Y., Chen, G., Reniers, G., 2020. Vulnerability assessment of atmospheric storage tanks to floods based on logistic regression. Reliab. Eng. Syst. Saf. 196, 106721.
Yin, Y., Zhang, X., Lin, D., Yu, H., Wang, J., Shi, P., 2014. GEPIC-V-R model: a GIS-based tool for regional crop drought risk assessment. Agric. Water Manag. 144, 107–119.
Yu, H., Shen, Y., Kelly, R., Qi, X., Wu, K., Li, S., Yu, H., Bao, X., 2020. Trends in social vulnerability to storm surges in Shenzhen, China. Nat. Hazards Earth Syst. Sci. 20 (9), 2447–2462.
Yue, Y., Li, J., Ye, X., Wang, Z., Zhu, A.X., Wang, J., 2015. An EPIC model-based vulnerability assessment of wheat subject to drought. Nat. Hazards 78 (3), 1629–1652.
Yue, Y., Wang, L., Li, J., Zhu, A., 2018. An EPIC model-based wheat drought risk assessment using new climate scenarios in China. Clim. Chang. 147 (3–4), 539–553.

Zeng, Z., Wu, W., Li, Z., Zhou, Y., Guo, Y., Huang, H., 2019. Agricultural drought risk assessment in Southwest China. Water 11 (5), 1064.
Zhang, F., Chen, Y., Zhang, J., Guo, E., Wang, R., Li, D., 2019. Dynamic drought risk assessment for maize based on crop simulation model and multi-source drought indices. J. Clean. Prod. 223, 100–114.
Zhu, X., Hou, C., Xu, K., Liu, Y., 2020. Establishment of agricultural drought loss models: a comparison of statistical methods. Ecol. Indic. 112, 106084.